Geomechanics and Engineering, *Vol. 41, No. 2 (2025) 265-274*
https://doi.org/10.12989/gae.2025.41.2.265

Prediction of resilient modulus on unsaturated geomaterials via DEM modeling

Hyun-Su Park[a], Byeong-Su Kim[b] and Seong-Wan Park[*]

Departement of Civil and Environmental Engineering, Dankook University, 152, Jukjeon-ro, Sugi-gu, Gyeonggi-do, 16890, Republic of Korea

(*Received December 4, 2024, Revised April 9, 2025, Accepted April 11, 2025*)

Abstract. Soil suction and the degree of saturation influence the resilient modulus, which should be considered when designing road and railway foundations. To reasonably account for these factors, a suction stress model incorporating both suction and degree of saturation was established for application in transportation design. In this study, the suction stress was considered by categorizing water into bulk and meniscus water and applying cyclic loading to the samples. The soil water characteristic curve (SWCC) was generated using discrete element method (DEM) analysis. Additionally, the resilient modulus was observed to vary with both deviator stress and the degree of saturation. The trends observed in this study are consistent with the results of laboratory tests conducted by other researchers. These findings demonstrated that the water division and cyclic loading algorithm effectively represented the unsaturated soil state. Furthermore, DEM analysis revealed that the suction stress was influenced the resilient modulus, with the resilient modulus increasing as suction stress increased.

Keywords: discrete element method; resilient modulus; suction stress; unsaturated soil state

1. Introduction

Deformation of foundation layers under cyclic traffic loads is an important parameter for evaluating pavement performance. The resilient modulus, which is the ratio of the repeated deviator stress to the axial strain, is widely used to evaluate foundation deformation. It is affected by factors such as deviator stress, confining stress, density, and suction (Lekarp *et al.* 2000). Changes in suction due to seepage from the pavement surface or rising groundwater level affect the resilience modulus. Edil and Motan (1979) and Yang *et al*. (2008) reported that the resilient modulus increases and decreases in the low and high suction range respectively, because suction increases the effective stress of the specimen. In addition, the relationship between suction and resilient modulus can be reasonably predicted by considering the moisture regime, which refers to the volumetric water content or degree of saturation (Han *et al.* 2016). Suction stress can be derived from suction and effective saturation and is used to predict shear strength in unsaturated soil mechanics (Karube *et al.* 1986). Thus, the suction stress can be used to predict resilient modulus, but the relationship between suction stress and resilient modulus is still not properly understood.

Various tests can be used to evaluate the effect of suction on the resilient modulus with the filter paper, axis-translation method, and vapor pressure methods. The commonly used filter paper method measures suction after the test (Zhang *et al.* 2019). The filter paper method is simple but highly user-dependent and unreliable (Ng and Menzies 2014). The axis-translation method can control suction, but it is unsuitable for applications involving high suction due to the limitation of high air entry in the ceramic disk (Salour *et al.* 2014). To solve these problems, Banerjee *et al*. (2020) proposed a vapor pressure method that can control suction up to 500 MPa. However, this method takes 2 weeks to reach the target suction. Therefore, evaluating the influence of suction on the shear behavior of unsaturated soils under high suction conditions remains a challenge task.

Discrete element method (DEM) analysis has recently been used to overcome the limitations of laboratory tests in geotechnical engineering (Hussain and Hussaini 2023, Kodicherla 2023, Zang *et al.* 2024). Yohannes *et al*. (2014) used DEM analysis to evaluate the effect of particle properties on resilient modulus. Similarly, Arulrajah *et al.* (2020) used DEM analysis to evaluate the effect of recycled concrete aggregates on resilient modulus. To determine the resilient modulus of unsaturated soils, it is necessary to consider the effect of the degree of saturation. Consequently, DEM simulation-based unsaturated soil modeling is required to capture the change in resilient modulus according to the degree of saturation.

Additionally, since suction stress is determined by both suction and water content, it is essential to model both suction and water content in DEM to incorporate suction stress. Liu and Sun (2002) and Li *et al.* (2018) proposed analytical methods for unsaturated soils. These researchers evaluated the shear behavior of unsaturated soils by applying capillary forces between particles under low degrees of saturation conditions. Recently, Suh (2024)

*Corresponding author, Professor
E-mail: spark@dankook.ac.kr
[a]Ph.D., Postdoc. Researcher
[b]Associate Professor

ISSN: 2005-307X (Print), 2092-6219 (Online)

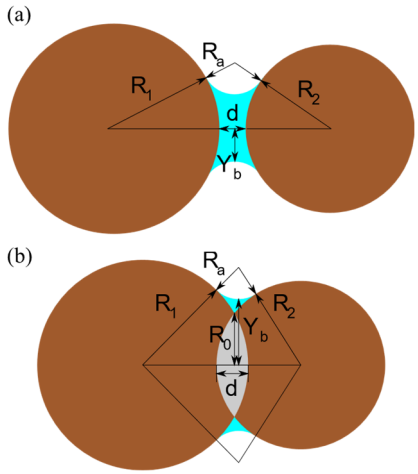

Fig. 1 Water volume calculation method: (a) when the particles are separated: (b) when the particles overlap. R_1 and R_2 are the radii of the particles, R_0 is the length of the secant line that connects the intersection points of two particles (i.e., common chord), R_a is the radius of the air, d is the length of particle to particle, and Y_b is the radius of the fluid neck that connects the two particles

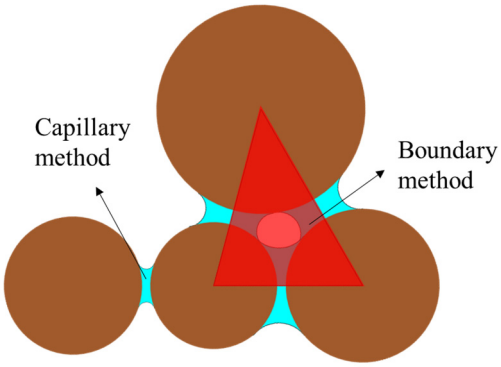

Fig. 2 Method for applying general capillary and boundary forces between particles in unsaturated soil simulations

performed a triaxial test involving DEM analysis at low degrees of saturation levels. However, pore water is classified into two types: meniscus water and bulk water (Karube *et al.* 1996). Meniscus water exists at the contact points between two particles. As its volume increases, adjacent meniscus waters coalesce. The resulting water occupies the pore volume formed by at least three particles and is termed bulk water (Wang *et al.* 2017). At low degree of saturation, only meniscus water is considered. Whereas under higher degree of saturation both meniscus and bulk water must be taken into account. Liu *et al.* (2020) simulated higher degree of saturation by modeling water volume coalescence; however, this approach requires additional analysis to quantify the resulting water volume. Although more accurate that other methods, this approach is time-consuming. To simulate the shear behavior in an unsaturated state during particle deformation under loading, it is necessary to represent the virtual water present between the particles using mathematical relationships and to calculate and apply the corresponding capillary forces.

This study aims to simulate the behavior of unsaturated soil using DEM analysis (PFC 3D). To achieve this, the water content in unsaturated soils was divided into bulk and meniscus water, and cyclic loading was applied to the specimen to evaluate the effect of suction on resilient modulus. Additionally, a soil-water characteristic curve (SWCC) and resilient modulus were generated through DEM simulation. From these results, the effect of suction stress on resilient modulus was evaluated.

2. Unsaturated resilient modulus through DEM analysis

2.1 Definition of suction stress

Suction stress is related to suction and the degree of saturation (Karube and Kato 1994) and has been evaluated through triaxial compression, unconfined compression, and direct shear tests. It represents the effect of suction on the mechanical behavior of unsaturated soils under various stress states. Suction stress is defined as the sum of bulk and meniscus stress, and can be calculated as the product of suction and effective degree of saturation as follows (Karube and Kato 1994)

$$p_s = p_m + p_b = \frac{S_r - S_{r0}}{100 - S_{r0}} \cdot s \quad (1)$$

where p_m = the meniscus stress (kPa), p_b = the bulk stress (kPa), Sr = the degree of saturation (%), S_{r0} = the residual degree of saturation (%), and s = the matric suction (kPa).

Bulk stress refers to the stress imposed on pores filled with water, whereas meniscus stress refers to the stress imposed by the capillary force. Bulk and meniscus water cannot be directly separated in laboratory tests due to their microscopic nature. Karube and Kawai (2001) conceptually predicted the driest curve, defined as the soil-water characteristic curve without bulk water in the pore water. However, it is impossible to separate them experimentally.

2.2 Modeling of unsaturated state in DEM analysis

The unsaturated state was modeled through four stages of DEM analysis. First, the volume of water for particle-to-particle interaction was defined based on the particle-to-particle spacing (d) as shown in Fig. 1. The radius of the fluid neck connecting the two particles (Y_b) is assumed to be N times the radius of the smaller particle (R_2) among the two particles. Using this fluid neck radius, the radius of the air can be determined by assuming that the air forms a circle. The water volume is calculated based on the radii of the fluid neck, the air, the large and small particles, and the distance between the particles. This calculation is divided into three cases. First, when the particles are separated (Fig. 1(a)), the water volume is determined using geometric methods. Second, when the particles overlap and the length of the secant line (R_0) is smaller than the fluid neck radius

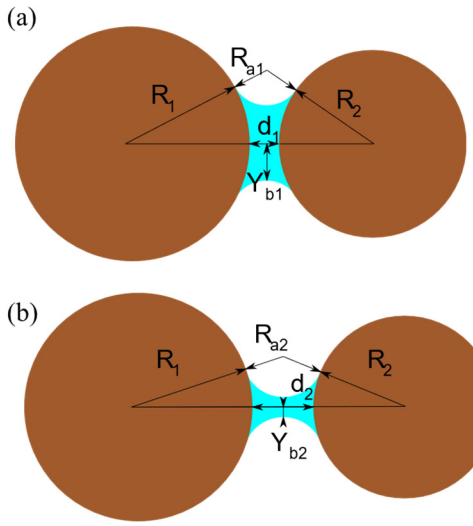

Fig. 3 Change in water volume when particles move apart: (a) state before particle movement and (b) state after particle movement

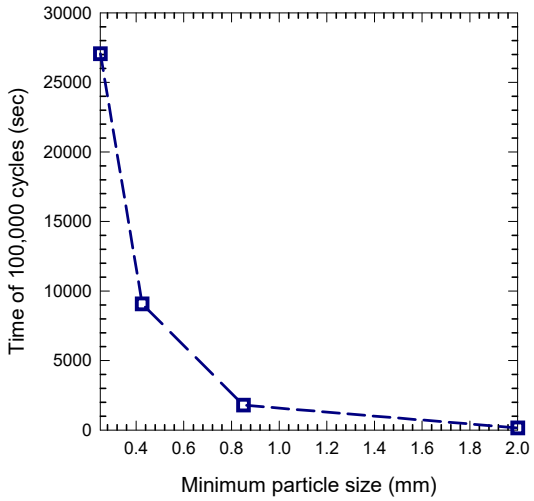

Fig. 4 Computational time per 100,000 cycles with respect to minimum particle size

(Y_b) (Fig. 1(b)), the water volume is calculated by considering the overlapping volume using geometric methods. Third, when the particles overlap but the length of the secant line (R_0) is larger than the fluid neck radius (Fig. 1(b)), the water volume is not calculated. From these calculations, the degree of saturation is computed based on the water volume, and its variation with different fluid neck radii is expressed by Eq. (2). The desired degree of saturation is determined by the value of N, which is the ratio of radius of fluid neck to radius of smaller particle. For example, a value of N equal to 0.62 corresponds to a degree of saturation of 40%.

$$S_r = 7.6N^5 - 28.9N^4 + 36.7N^3 + 18.2N^2 + 4.2N - 0.3 \quad (2)$$

where, S_r is the degree of saturation (m^3/m^3), and N is the ratio of radius of fluid neck to radius of smaller particles.

Second, water in particle interactions was classified into bulk and meniscus water according to the volume of water. The pore water of soil materials was classified into bulk and meniscus water (Karube *et al.* 1996). Bulk and meniscus water were separated because overlapping water was defined as bulk water. However, not all overlapping water was considered bulk water, and bulk water is defined as the water that fills pores. Therefore, bulk water is defined as the water overlapping within the triangle area formed by three particles. For example, when three particles form a triangle and water exists between particles A and B, A and C, and B and C, if all three waters overlap, it is classified as bulk water, and the remaining water is classified as meniscus water.

Third, different capillary forces were applied depending on the type of water. Because meniscus water does not overlap, the general capillary force method, which calculates the sum of the axial surface tension and the hydrostatic force at the water neck, can be applied. However, determining the neck of water in bulk water is difficult. Instead, the boundary method was proposed by Hotta *et al.* (1984) and applied to bulk water by Murase *et al.* (2008). The capillary force of the boundary method was calculated from the filling angle at the contact line. Therefore, the capillary force calculated using the general capillary force method was applied to meniscus water, and the capillary force calculated using the boundary method was applied to bulk water (Fig. 2).

Finally, the water thickness was adjusted according to the deformation of the particles. The water volume defined in the first step should be maintained throughout the shear process. However, as shown in Fig. 3, particle deformation during shearing increases the spacing between particles from d_1 to d_2. Because water cannot be lost during shearing, the total water volume remains constant. Consequently, as particle spacing increases, the radius of the air (R_a) increases from R_{a1} to R_{a2}, while the radius of the fluid neck (Y_b) decrease from Y_{b1} to Y_{b2}. The optimal neck radius and air radius can be determined iteratively using several optimization methods. The Newton-Rapson method is accurate and commonly used for optimization, but it is time-consuming. The secant method is potentially the fastest optimization method, and it is used to determine the size the neck of water based on the distance between particles (Quarteroni *et al.* 2010). Thus, the neck of water was determined using the secant method in this study.

2.3 Modeling of cyclic loading condition

The stress state of the resilient modulus test is classified into confining stress and deviator stress. Li *et al.* (2017) proposed a membrane modeling method to keep the confining pressure constant. This method is divided into two parts. First, the position vector of the membrane particle is calculated from the ball position. Second, the area of each particle in the membrane is calculated from nearby particles. The force applied to the ball is calculated from the position vector and the area, and it is applied to the ball. Using this method, the confining pressure can be kept constant.

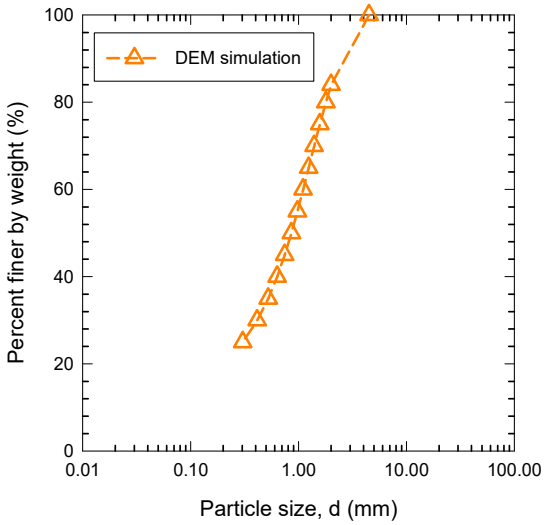

Fig. 5 Particle size distribution

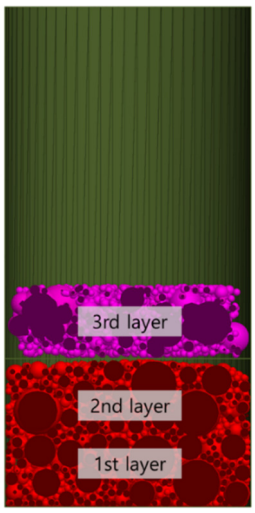

Fig. 6 Compaction scenario during the generation of 3rd layer

Table 1 Contact model properties

Parameters	Value
Membrane particles	
Effective modulus (kN/m)	600
Normal to shear stiffness ratio	0
Friction coefficient	0
Damping ratio	0.7
Density (kg/m^3)	1
Membrane-to- specimen particles and platen-to-specimen particles	
Effective modulus (kN/m)	6000
Normal to shear stiffness ratio	0
Friction coefficient	0
Damping ratio	0.7
Specimen particles	
Effective modulus (kN/m)	6000
Normal to shear stiffness ratio	1.2
Friction coefficient	0.5
Damping ratio	0.7
Density (kg/m^3)	2.69
Maximum void ratio, e_{max}	0.417
Minimum void ratio, e_{min}	0.360
Void ratio, e	0.360
Relative density, D_r (%)	100

The haversine form of cyclic loading is commonly used in the resilient modulus test. Haversine loading involves applying a small increment of loading force in the initial loading sequence, and the loading force is increased gradually along the loading sequence. In DEM analysis, because a specific load cannot be applied directly to a material such as a wall, the loading pressure is usually controlled by adjusting the wall velocity. Therefore, the haversine load was applied to the wall boundary with deformation control for the DEM analysis. For the cyclic loading pressure to reach the target value, the haversine-shaped load magnitude was gradually generated, and the velocity was appropriately adjusted according to the generated haversine load.

3. Modeling method of resilient modulus test

The simulation time in DEM simulations varies depending on the number of particles. To address this, the particle size or simulation specimen size is often scaled in DEM simulations to mitigate the increase in simulation time caused by more particles (Li *et al.* 2018, Kuhn and Daouadji 2020). To determine the appropriate simulation time, we examined the time required to complete 100,000 cycles for various minimum particle size (i.e., 0.25, 0.425, 0.85, 2 mm). Fig. 4 illustrates the relationship between simulation time and the minimum particle size. Noticeably, the simulation time increases as the minimum particle size decreases. For minimum particle size of 0.25 and 0.425 mm, the number of particles is 27,079 and 9,101, respectively. If the minimum particle size is less than 0.25 mm, the simulation will take a long time to complete. Therefore, for a practical and efficient simulation, approximately 20,000 particles can reasonably be used. In this study, to minimize the influence of the maximum particle size, the specimen size was set to at least six times the maximum particle size. Additionally, the smallest particle size was adjusted to ensure that the total number of particles reached approximately 20,000. The particle size distribution applied is shown in Fig. 5.

In DEM simulations, particles are modeled as spherical balls, resulting in a particle shape and particle size distribution that differs from those of actual soil materials. This discrepancy means that the interlocking effect between particles is absent, and the simulated density does not correspond to the real density. To address the interlocking

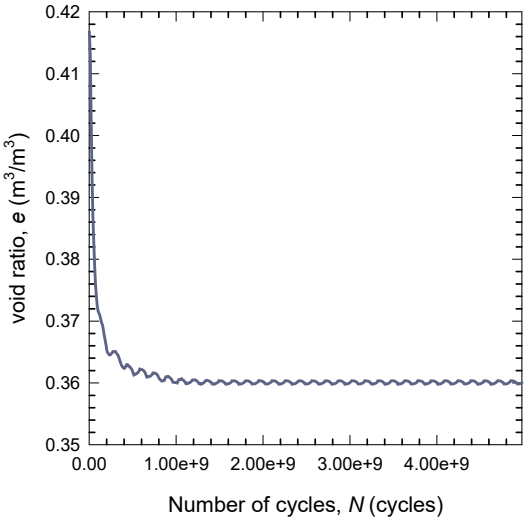

Fig. 7 Change in void ratio with the number of cycles as obtained through the compaction algorithm

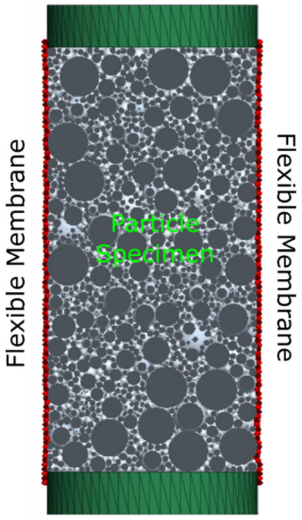

Fig. 8 Modeling of specimen and membrane particles

effect, some researchers have introduced particle friction (Shen *et al*. 2016). In density modeling using particle friction, the friction is employed to control the specimen's density. For the loose specimen, the particle friction coefficient is set to 1.0, whereas for the dense specimen, it is set to 0.0. However, this method remains inefficient, as it still fails to accurately replicate the actual material density. In this study, the density modeling method proposed by Chang *et al*. (2017) was utilized to determine the maximum and minimum void ratio of the simulated material. This density modeling method applies ASTM D 4253 to obtain the minimum void ratio. The soil particles are generated within a mold with rigid boundary walls (diameter: 152.4 mm, height: 155.2 mm). A seating load of 13.8 kPa is applied to the specimen, followed by vertical vibration. The maximum and minimum void ratios obtained through this method were then used to effectively simulate the density effect in DEM simulations.

The density modeling method in this study involves the following. First, particles are arranged within a box. When generating new particles, the particles are placed as close as possible to the top of the already generated particles, because if particles are generated far above the top layer, the generated particles fall onto the generated particles over a longer period. As the falling time increases, the particles gain higher velocities due to gravitational effects. To minimize the impact of gravity, particles are generated a short distance above the top of the generated particles. Fig. 6 illustrates this process. The first and second layers are arranged, and the 3rd layer represents the initial state of particle arrangement. The generated particles are then allowed to move until their velocities are approximately.

After particles generation, the maximum void ratio was determined based on the initial void ratio. Subsequently, a pressure of 13.8 kPa was applied to the top of the specimen to apply compaction. To simulate the effects of a vibration table, vertical vibrations at a frequency of 60 Hz were applied to the bottom of the specimen. Fig. 7 illustrates the relationship between the void ratio and the number of cycles. Noticeably, the void ratio decreases gradually and stabilizes to a specific value.

The specimen used for DEM analysis is shown in Fig. 8. The sample has a diameter of 10 mm and a height of 20 mm, with particle size ranging from 0.3031 mm to 2.0 mm. After the specimen was compacted to achieve the target void ratio, the membrane surrounding the specimen was modeled using spherical particles (membrane balls). Selecting an appropriate membrane ball size is crucial for maintaining computational efficiency and accuracy. If the membrane balls are too small, the analysis time increases significantly due to the large number of balls. However, if the membrane balls are too large, controlling the confining pressure accurately becomes difficult, and the error in volume change increases. According to Qu *et al*. (2019), the ratio of the specimen diameter to the membrane particle should be greater than 35. When the ratio is greater than 35, the error is less than 5%, but when it is around 33, the error is about 6-7%. Based on these results, the size of the membrane ball was set to be equal to the minimum particle size of the specimen, and the radius ratio was set to 33.

The contact properties of membrane particles, membrane-to-specimen particles, platen-to-specimen particles, and specimen particles are summarized in Table 1. The effective modulus of the specimen particles is set to 6,000 kN/m, and the effective modulus of membrane particles is set to one-tenth the effective modulus of the specimen particles. If the effective modulus of membrane particles is too small, the membrane particles may penetrate into the specimen. However, If the effective modulus of the membrane particles is too large, the specimen particles may lose alignment and thus, stability (De Bono *et al.* 2012). Therefore, the effective modulus of membrane particles was determined through a trial-and-error approach.

The resilient modulus, as defined by Seed *et al.* (1962), is the ratio of deviator stress to recoverable strain as follows.

$$M_r = \sigma_d / \varepsilon_r \tag{3}$$

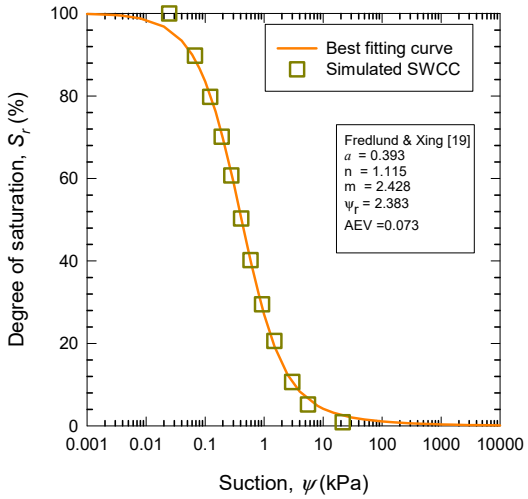

Fig. 9 Soil-water characteristic curve generated through DEM analysis

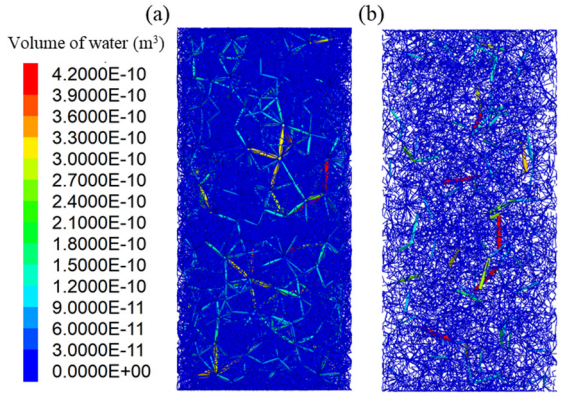

Fig. 10 Water volume at contact point for S_r= 70%: (a) Bulk water and (b) Meniscus water

where, M_r is the resilient modulus (kPa), σ_d is the deviator stress (kPa), ε_r is the recoverable strain ($\varepsilon_r = \Delta L/L$), ΔL is the recoverable deformation, and L is the original sample length. Because each loading cycle in DEM simulations requires approximately one-hour, resilient modulus in this study was calculated using only five loading cycles under each condition. Comparisons between the resilient modulus and both degree of saturation and stress conditions were performed using the value obtained at the fifth cycle.

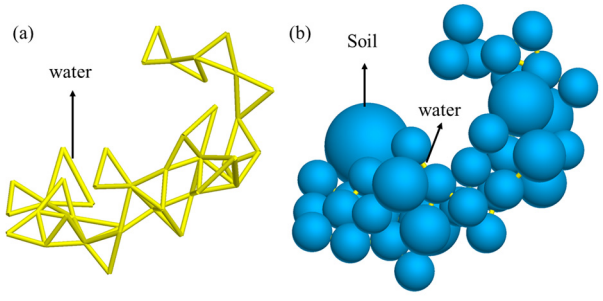

Fig. 11 Specific bulk water contact in soil: (a) bulk water contact and (b) bulk water contact represented by balls

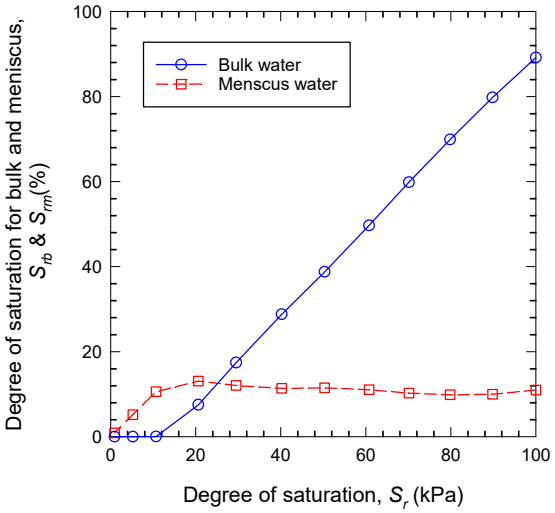

Fig. 12 Changes in bulk and meniscus water with respect to the degree of saturation

Table 2 Maximum and minimum resilient modulus

No.	1	2	3
Confining stress, σ_c (kPa)	27.6	27.6	27.6
Deviator stress, σ_d (kPa)	13.8	41.4	68.9
Maximum resilient modulus, M_{rmax} (MPa)	4.09	3.99	3.04
Minimum resilient modulus, M_{rmin} (MPa)	4.08	3.98	2.99

4. SWCC and resilient modulus at various suctions

In DEM analysis, suction was calculated based on the water distribution between particles using the proposed unsaturated soil modeling method. Consequently, the relationship between suction and degree of saturation (S_r), referred to as the soil water characteristic curve (SWCC), was generated through DEM simulations, as shown in Fig. 9.

The degree of saturation begins to decrease at approximately 0.1 kPa of suction and decreases sharply between 0.1 kPa and 3 kPa of suction. Beyond this range, the degree of saturation stabilizes near zero at approximately 10 kPa of suction. Additionally, the generated SWCC includes key characteristics such as the air entry value (AEV) and residual suction. These results reveals that the shape of the generated SWCC closely resembles that of SWCCs obtained from laboratory test. These results demonstrate that the proposed unsaturated soil modeling method effectively simulate the relationship between suction and the degree of saturation.

The proposed water distribution algorithm, can be used to categorize the water content into bulk and meniscus water. Fig. 10 illustrates the distribution of bulk and meniscus water at S_r= 70%. Noticeably, the bulk water contacts are more extensive than the meniscus water contacts, and the volume of bulk water exceeds that of the meniscus water at S_r= 70%. Additionally, Fig. 11 highlights the bulk water contacts in the soil. The bulk

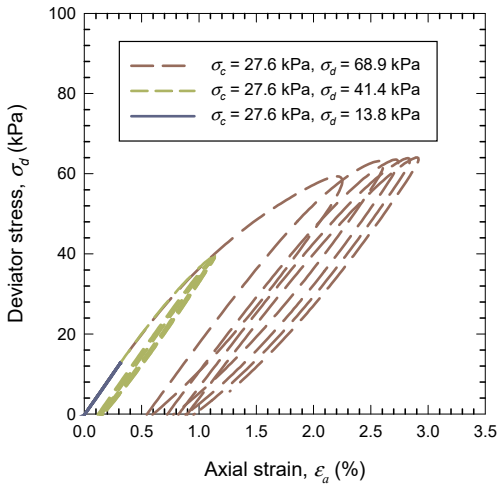

Fig. 13 Relationship between deviator stress and axial strain under varying deviator stress levels at S_r= 1%

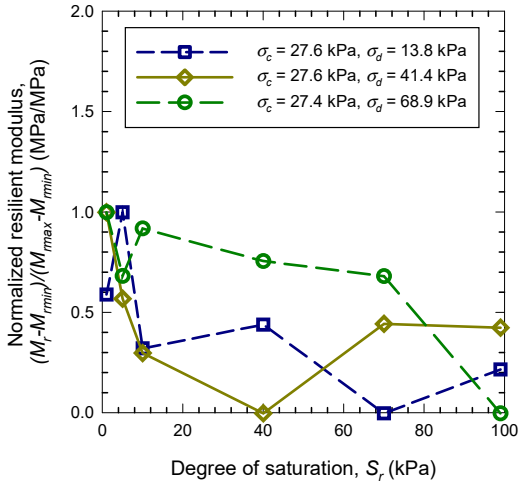

Fig. 14 Changes in normalized resilient modulus with respect to the degree of saturation

water tends to occupy triangular contact regions between particles. Notably, bulk water often spans multiple particles, forming larger bulk water clusters. These observations indicate that the proposed algorithm effectively distinguishes between bulk water and meniscus water in unsaturated soils.

Fig. 12 illustrates the changes in bulk and meniscus water with the degree of saturation. To investigate the variation in bulk and meniscus water with the degree of saturation, The ratio of bulk to meniscus water changes significantly at approximately S_r= 25%. When the total degree of saturation is below 25%, the amount of meniscus water exceeds that of bulk water. However, when the total degree of saturation exceeds 25%, bulk water dominates over the meniscus water. Additionally, when the total degree of saturation surpasses 20%, the amount of meniscus water remains nearly constant, with negligible variation up to approximately S_r= 10%

Karube and Kawai (2001) divided the bulk and meniscus water using the bounding wetting curve, as determined by the boundary of the wetting curve. In their study, the meniscus water remained at approximately at approximately S_r= 10%, and exhibited behavior consistent with that depicted in Fig. 12. Therefore, the proposed water division model for bulk and meniscus water aligns with the laboratory test results. Therefore, the water division modeling approach is appropriate for simulating unsaturated soil behavior.

Fig. 13 illustrates the relationship between deviator stress and axial strain under varying deviator stress conditions at S_r= 1%. The confining stress was kept constant at 27.6 kPa, as deviator stresses of 13.8 kPa, 41.4 kPa, and 68.9 kPa were applied. The degree of saturation was set to 1, 5, 10, 40, 70, and 99%. This condition was chosen because suction stress decrease beyond approximately S_r= 10%, leading to variations in the resilient modulus. Fig. 14 illustrates the relationship between the degree of saturation and the resilient modulus.

The difference in resilient modulus is minimal because the effective modulus of the particles was set to a small value to reduce the computational time. Although the computational time for one cycle depends on the degree of saturation, it is approximately 1 hour. Table 2 presents the maximum and minimum resilient moduli for varying deviator stress levels. When the deviator stress is 13.8 kPa, the difference in resilient modulus with changes in the degree of saturation is minimal.

To analyze the resilient modulus, it was normalized using its maximum and minimum values. This normalization scaled the resilient modulus to a range between 0 and 1. Table 2 presents the maximum and minimum resilient moduli. Noticeably, the resilient modulus decreases as the deviator stress increases. This trend is consistent with previous findings that the resilient modulus decreases with increasing deviator stress (Ng *et al*. 2013, Han and Vanapalli 2016). As listed in Table 2, both the maximum and minimum resilient moduli decrease as the deviator stress increases.

Additionally, resilient modulus varies with the degree of saturation. Specifically, resilient modulus increases as the degree of saturation decreases. Banerjee *et al*. (2020) conducted resilient modulus tests over a wide range of degree of saturation and found that resilient modulus increases as the degree of saturation decreases, with the slope decreasing at low degree of saturation. As illustrated in Fig. 14, resilient modulus increases as the degree of saturation decreases.

However, the resilient modulus in this study was relatively small, and a partial decrease was observed as the degree of saturation increased. This is attributable to the resilient modulus being determined after only 5 cycles, whereas it is typically determined after 100 cycles. Due to computational constraints, the resilient modulus was calculated after five cycles, resulting in less stable values. Despite this limitation, the overall trend in the relationship between resilient modulus and degree of saturation aligns closely with the results reported by other researchers. Therefore, the proposed algorithm effectively simulates the effects of deviator stress and degree of saturation on the resilient modulus.

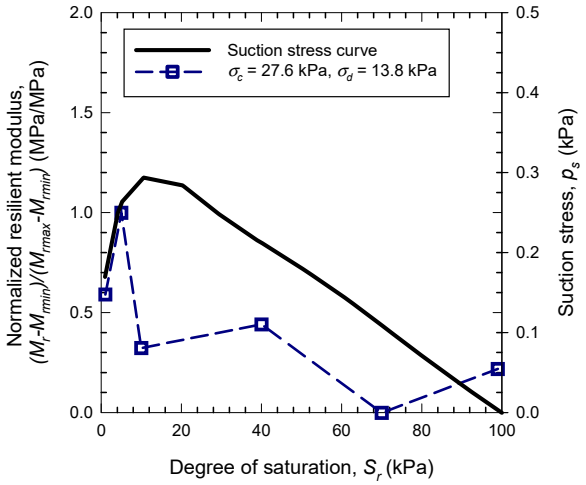

(a) deviator strsss of 13.8 kPa

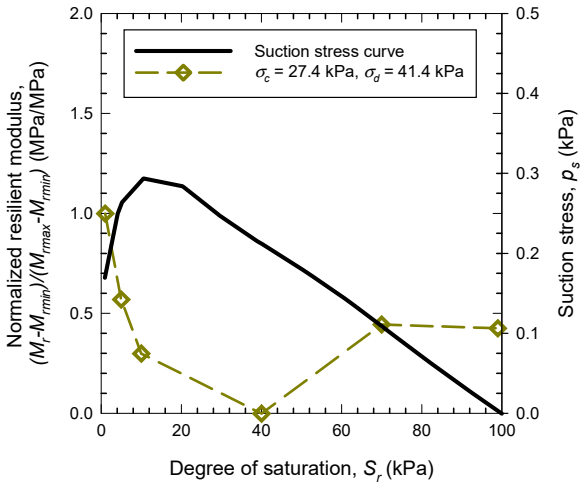

(b) deviator strsss of 41.4 kPa

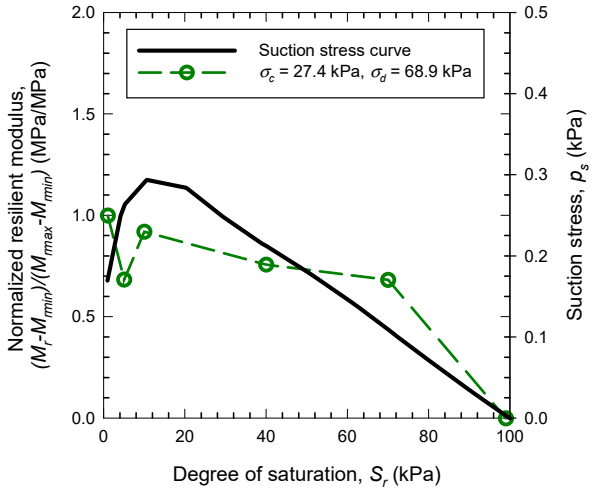

(c) deviator strsss of 68.9 kPa

Fig. 15 Comparison between normalized resilient modulus and suction stress under various deviator stress levels

Fig. 15 illustrates the relationship between resilient modulus and degree of saturation and that the relationship between suction stress and degree of saturation. To verify the effects of suction stress, the changes in resilient modulus with the degree of saturation were compared to the variations in suction stress. Suction stress was calculated using Eq. (1) based on the generated SWCC.

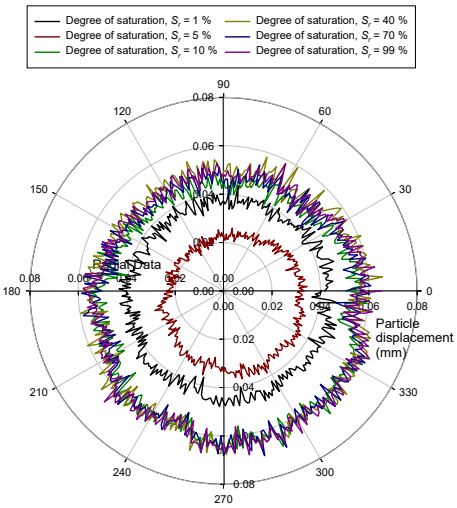

Fig. 16 Particle displacement depending on the degree of saturation (Confining stress = 27.8 kPa, Deviator stress = 13.8 kPa)

At high degree of saturation, suction stress increased as the degree of saturation decreased. However, at low approximately S_r= 10%, the suction stress decreased as the degree of saturation decreased. This behavior occurs because, at low degree of saturation, the water volume is relatively small, resulting in suction stress decreasing as the degree of saturation increases.

When the relationship between the degree of saturation and suction stress was compared with the normalized resilient modulus results, the resilient modulus at a deviator stress of 13.8 kPa demonstrated a strong correlation with suction stress. The resilient modulus increases with suction stress as the degree of saturation decreases from 99% to 5%, but then decreases as saturation further declines from 5% to 1%. This pattern indicates that the resilient modulus varies with changes in suction stress, demonstrating a relationship between suction stress and resilient modulus. However, under higher deviator stress conditions, the resilient modulus increased even as suction stress decreased at low degree of saturation. This occurs because the suction stress (< 0.3 kPa) is much smaller than the applied deviator stress (> 41.4 kPa). In our simulation, neither contact angle nor fine particles were considered, resulting in relatively low suction stress values. Under lower deviator stress conditions, however, a clear relationship between resilient modulus and suction stress was observed. Therefore, the water partitioning algorithm and contact model may require revision to improve accuracy.

Fig. 16 illustrates the displacement of specimen particles extracted using DEM simulation. The size and direction of displacement were calculated, and displacements in the same direction were averaged. Noticeably, the displacement at S_r= 5% is the smallest and the displacements at a degree of saturation above 10% are similar. However, particle

displacement increases again at S_r= 1%, showing a trend similar to suction stress. The deformation behavior is affected by the suction stress and water distribution. When the saturation is more than 10% or less than 1%, the deformation is large because the suction stress is low. On the other hand, at the degree of saturation of 5%, the deformation is small because the suction stress is higher than other conditions. In addition, when the degree of saturation is more than 10%, the proportion of bulk water is higher than that of meniscus water, which leads to a large deformation. Similarly, when the degree of saturation is less than 1%, only a small amount of meniscus water exists in the pores, which also causes a large deformation. In summary, it can be concluded that at the degree of saturation of 5%, most of the water exists as meniscus water, which helps to reduce the deformation. These results indicate that particle displacement is related to suction stress.

5. Conclusions

This study divided the water contents into bulk and meniscus water to simulate unsaturated soils. Cyclic loading was then applied to a specimen consisting of bulk and meniscus water. The resilient modulus was then obtained from these simulations. The observation and findings from the simulation are summarized as follows:

(1) Based on the particle size distribution, the SWCC was generated through DEM simulation. The distribution of bulk and meniscus water varied with the total degree of saturation: bulk water was dominant at a degree of saturation above 25%, whereas meniscus water was dominant below 25%. These results demonstrate that the unsaturated soil state can be effectively simulated using DEM analysis despite its limitations.

(2) The resilient modulus was obtained through DEM simulation, and it decreased as the deviator stress increased from 13.8 kPa to 68.9 kPa. These results indicate that the simulated unsaturated soil can effectively accommodate cyclic loading.

(3) The suction stress was compared with the resilient modulus. The trend of suction stress with the degree of saturation changed at S_r= 10%, whereas particle displacement changed at S_r= 5%. Although the relationship between suction stress and resilient modulus remains unclear due to DEM simulation limitations, suction stress was found to influences the resilient modulus. This effect can be further clarified through algorithm revisions.

(4) An unsaturated modeling approach that considers the range of low to high suction under limited conditions is proposed, which allowed simulating the shear behavior of unsaturated soil materials under various unsaturated conditions.

Acknowledgments

This work was supported by the National Research Foundation of Korea (NRF) grant funded by the Korea government (MSIT) (No. RS-2023-00221184).

References

Arulrajah, A., Baghban, H., Narsilio, G.A. and Horpibulsuk. (2020), "Discrete element analysis of recycled concrete aggregate responses during repeated load triaxial testing", *Transport. Geotech.*, **23**, 100356. https://doi.org/10.1016/j.trgeo.2020.100356.

Banerjee, A., Puppala, A.J., Hoyos, L.R., Likos, W.J. and Patil, U.D. (2020), "Resilient modulus of expansive soils at high suction using vapor pressure control", *Geotech. Test. J.*, **43**(3), 720-736. https://doi.org/10.1520/GTJ20180255.

Chang, C.S. Deng, Y. and Yang, Z. (2017), "Modeling of minimum void ratio for granular soil with effect of particle size distribution", *J. Eng. Mech.*, **143**(9), 04017060. https://doi.org/10.1061/(ASCE)EM.1943-7889.0001 270.

De Bono, J. McDowell, G. and Wanatowski, D. (2012), "Discrete element modelling of a flexible membrane for triaxial testing of granular material at high pressures", *Géotechniqu Lett.*, **2**(4), 199-203. https://doi.org/10.1680/geolett.12.00040.

Edil, T.B. and Motan, S.E. (1979), "Soil-water potential and resilient behavior of subgrade soils", *Transportation Research Record: Transportation Research Board*, **705**, 54-63.

Han, Z. and Vanapalli, S.K. (2016), "State-of-the-art: Prediction of resilient modulus of unsaturated subgrade soils", *Int. J. Geomech.*, **16**(4), 04015104. https://doi.org/10.1061/(ASCE)GM.1943-5622.0000631.

Hotta, K., Takeda, K. and Iionya, K. (1974), "The capillary binding force of a liquid bridge", *Powder Technol.*, **10**, 231-242. https://doi.org/10.1016/0032-5910(74)85047-3.

Hussain, M. and Hussaini, S.K.K. (2023), "Effects of normal stress, shearing rate, PSD and sample size on behavior of ballast in dicrect shear tests using DEM simulation", *Geomech. Eng.*, **35**(5), 475-486. https://doi.org/10.12989/gae.2023.35.5.475.

Karube, D., Kato, S. and Katsuyama, J. (1986), "Effective stress and soil constants of unsaturated kaolin", *Doboku Gakkai Ronbunshu*, **370**(5), 179-188. (In Japanese) https://doi.org/10.2208/jscej.1986.370_179.

Karube, D., Kato, S., Hamada, K. and Honda, M. (1996), "The relationship between the mechanical behavior and the state of pore-water in unsaturated soil", *Doboku Gakkai Ronbunshu*, **535**, 83-92. (In Japanese). https://doi.org/10.2208/jscej.1996.535_83.

Karube, D. and Kato, S. (1994), "An ideal unsaturated soil and the Bishop's soil", *Proceedings of the 13th international conference on conference on soil mechanics and foundations engineering*, New Delhi, India.

Karube, D. and Kawai, K. (2001), "The role of pore water in the mechanical behavior of unsaturated soils", *Geotech. Geol. Eng.*, **19**, 211-241. https://doi.org/10.1023/A:1013188200053.

Kodicherla, S.P.K. (2023), "Discrete element modelling of granular materials incorporating realistic particle shapes", *Int. J. Geo-Eng.*, **14**(15), 14 https://doi.org/10.1186/s40703-023-00193-y.

Kuhn, M.R. and Daouadji, A. (2020), "Simulation of undraind quasi-saturated soil with pore pressure measurements using a discrete element (DEM) algorithm", *Soils Found.*, **60**, 1097-1111. https://doi.org/10.1016/j.sandf.2020.05.013.

Lekarp, F., Isacsson, U. and Dawson, A. (2000), "State of the art. I: resilient response of unbound aggregates", *J. Transport. Eng.*, **126**(1), 66-75. https://doi.org/10.1061/(ASCE)0733-947X(2000)126:1(66).

Li, Z., Wang, Y.H., Ma, C.H. and Mok, C.M.B. (2017), "Experimental characterization and 3D DEM simulation of bond breakages in artificially cemented sands with different bond strengths when subjected to triaxial shearing". *Acta Geotech.*, **12**, 987-1002. https://doi.org/10.1007/s11440-017-0593-6.

Li, T., Jiang M. and Thornton, C. (2018), "Three-dimensional discrete element analysis of triaxial tests and wetting tests on unsaturated compacted silt", *Comput. Geotech.*, **97**, 90-102. https://doi.org/10.1016/j.compgeo.2017.12.011.

Liu, S.H. and Sun, D.A. (2002), "Simulating the collapse of unsaturated soil by DEM", *Int. J. Numer. Anal. Method. Geomech.*, **26**, 633-646. https://doi.org/10.1002/nag.215.

Liu, X., Zhou, A., Shen, S., Li, J. and Sheng, D. (2020), "A micro-mechanical model for unsaturated soils based on DEM", *Comput. Method. Appl. Mech. Eng.*, **368**, 113183. https://doi.org/10.1016/j.cma.2020.113183.

Murase, K. Mochida, T., Sagawa, Y. and Sugama, H. (2008), "Estimation on the strength of a liquid bridge adhered to three spheres", *Adv. Powder Technol.*, **19**, 349-367. https://doi.org/10.1163/156855208X314949.

Ng, C.W.W. and Menzies, B. (2014), "Advanced unsaturated soil mechanics and engineering", Taylor & Francis, London, UK.

Ng, C.W.W., Zhou, C., Yuan, Q. and Xu, J. (2013). "Resilient modulus of unsaturated subgrad soil: experimental and theretical investigations", *Can. Geotech J.*, **50**(2), 223-232. https://doi.org/10.1139/cgj-2012-0052.

Qu, T., Feng, Y.T., Wang, Y. and Wang, M. (2019), "Discrete element modelling of flexible membrane boundaries for triaxial test", *Comput. Geotech.*, **115**, 103154. https://doi.org/10.1016/j.compgeo.2019.103154.

Quarteroni, A., Riccardo, S. and Fausto, S. (2010), *Numerical mathematics*, Springer.

Salour, F., Erlingsson, S. and Zapata, C.E. (2014), "Modelling resilient modulus seasonal variation of silty sand subgrade soils with matric suction control", *Can. Geotech. J.*, **51**(12), 1413-1422. https://doi.org/10.1139/cgj-2013-0484.

Shen, Z., Jiang, M. and Thornton, C. (2016), "Shear strength of unsaturated granular soils: three-dimensional discrete element analyses", *Granular Matter.*, **18**(37), 1-13. https://doi.org/10.1007/s10035-016-0645-x.

Suh, H.S. (2024), "Evolution of anisotropic capillarity in unsaturated granular media within the pendular regime", *Int. J. Geo-Eng.*, **15**(10), 11. https://doi.org/10.1186/s40703-024-00211-7.

Wang, J., Gallo, E., Francois, B., Gabrieli, F. and Lambert P. (2017), "Capillary force and rupture of funicular liquid bridges between three spherical bodies", *Powder Technol.*, **305**, 89-98. https://doi.org/10.1016/j.powtec.2016.09.060.

Yang, S.R., Lin, H.D., Kung, J.H. and Huang, W.H. (2008), "Suction controlled laboratory test on resilient modulus of unsaturated compacted subgrade soils", *J. Geotech. Geoenviron. Eng.*, **134**(9), 1375-1384. https://doi.org/10.1061/(ASCE)1090-0241(2008)134:9(1375).

Yohannes, B., Tan, D., Khazanovich, L. and Hill, K.M. (2014), "Mechanistic modelling of tests of unbound granular materials", *Int. J. Pavement Eng.*, **15**(7), 584-598. https://doi.org/10.1080/10298436.2013.775442.

Zang, C., Jiang, B., Wang, X., Wang, H., Zhou, J., Chen, M. and Cong, Y. (2024), "Study on damage law and width optimization design of coal pillar with the discrete element method", *Geomech. Eng.*, **37**(6), 555-563. https://doi.org/10.12989/gae.2024.37.6.555.

Zhang, Y., Luo, X., Onifade, I., Huang, X., Lytton, R.L. and Birgisson, B. (2019), "Mechanical evaluation of aggregate gradation to characterize load carrying capacity and rutting resistance of asphalt mixture", *Constr. Build. Mater.*, **205**, 499-510. https://doi.org/10.1016/j.conbuildmat.2019.01.218.